energies

MDPI

Article

Comparative Analysis of Protection Schemes for Shunt Reactors: Addressing Turn-to-Ground and Turn Faults with Parametric Sensitivity and Transient Evaluations

Maria Leonor Silva de Almeida [1], Diogo Guilherme Ferreira [1], Lina P. Garcés Negrete [1], Jesús M. López-Lezama [2,*] and Nicolás Muñoz-Galeano [2]

[1] Electrical, Mechanical and Computer Engineering School, Federal University of Goiás, Av. Universitária No. 1488, Goiânia 74605-010, Brazil; marialeonor@ufg.br (M.L.S.d.A.); diogoguilherme@egresso.ufg.br (D.G.F.); lina_negrete@ufg.br (L.P.G.N.)

[2] Research Group in Efficient Energy Management (GIMEL), Departamento de Ingeniería Eléctrica, Universidad de Antioquia, Calle 67 No. 56-108, Medellin 050010, Colombia; nicolas.munoz@udea.edu.co

* Correspondence: jmaria.lopez@udea.edu.co

Abstract: In electrical power systems, shunt reactors control excess reactive power, keeping voltage levels within acceptable limits. As shunt reactors play a crucial role in the operation of electrical systems, it is essential to ensure the use of modern and fast protection schemes for these devices. Furthermore, protection functions must be capable of identifying various fault conditions, including critical operating situations such as turn-to-ground and turn faults, involving only a few short-circuited turns. This paper proposes a comparative evaluation of protection schemes commonly employed by manufacturers to meet the requirements of different grid codes. Thus, the investigation encompasses restricted earth fault, directional, differential, and distance functions. The latter is typically cited as a backup protection function. To support the analyses conducted, an electrical power system with shunt compensation was modeled in the ATPDraw software version 7.3. Through this platform, various internal fault conditions were simulated, encompassing turn-to-ground and turn faults. This facilitated the analysis of the influence of parameters such as the leakage factor value and the number of short-circuited turns. Additionally, external fault conditions were evaluated, including cases involving Current Transformer (CT) saturation.

Keywords: shunt reactor protection; turn-to-ground faults; turn faults; protection functions; parametric sensitivity analysis; ATPDraw simulations

Academic Editor: Marcin Kaminski

Received: 27 January 2025
Revised: 20 February 2025
Accepted: 21 February 2025
Published: 24 February 2025

Citation: de Almeida, M.L.S.; Ferreira, D.G.; Garcés Negrete, L.P.; López-Lezama, J.M.; Muñoz-Galeano, N. Comparative Analysis of Protection Schemes for Shunt Reactors: Addressing Turn-to-Ground and Turn Faults with Parametric Sensitivity and Transient Evaluations. *Energies* **2025**, *18*, 1097. https://doi.org/10.3390/en18051097

1. Introduction

1.1. Motivation

Electric Power Systems (EPSs) play a crucial role in modern society by providing the electricity needed to power homes, industries, and essential services. As global energy demand continues to rise, the efficient and reliable operation of EPSs becomes increasingly important. These systems must function within defined operational limits, such as voltage, frequency, and thermal constraints, to ensure stability and avoid equipment damage [1].

Additionally, EPSs are subject to environmental regulations aimed at reducing greenhouse gas emissions and minimizing the ecological impact of energy generation and transmission [2]. This means that modern power systems must not only work efficiently but also meet environmental standards [3].

Grid operators prioritize the safe and reliable operation of power systems to prevent blackouts and ensure uninterrupted service. They constantly monitor and control system

parameters to maintain the balance between electricity supply and demand while respecting technical and environmental constraints. One key technology that aids in voltage regulation and system stability is the shunt reactor. Shunt reactors are connected in parallel with transmission lines to absorb excess reactive power, counteracting the capacitive effects of long lines, particularly under low-load conditions [4]. Shunt reactors can be fixed or variable, allowing dynamic adjustments to meet changing network conditions, making them a critical component in modern power system management.

This necessity underscores the importance of deploying robust protection schemes capable of promptly identifying various fault types, including phase-to-phase faults, which occur when there is a short circuit between two phases; phase-to-ground faults, where one phase comes into contact with the ground or a grounded structure; turn-to-ground faults, which happen when a turn of a winding in a transformer or machine connects to the ground, often causing localized damage; turn faults, which involve short circuits between turns of the same winding and can lead to overheating and equipment failure; and three-phase faults, which are the most severe and involve a short circuit between all three phases [5].

While turn-to-ground and turn faults can also occur in other electrical equipment such as transformers, motors, and generators, this study focuses specifically on analyzing turn faults in shunt reactors. Consequently, the models and analyses presented are exclusively related to this type of equipment. Among the commonly employed protection functions for shunt reactors are differential elements, sequence overcurrent, sequence directional, and Restricted Earth Fault (REF) elements [6]. Although distance functions have traditionally been used as backup protection [7], recent research highlights their potential as primary protection mechanisms for reactors, offering an alternative approach to enhance fault detection and system reliability.

1.2. Related Work

Several studies have addressed the challenges of fault detection in shunt reactors, particularly in identifying turn-to-ground and turn faults, which often generate negligible fault currents. Li et al. [8] and Uriondo et al. [9] explored methodologies to enhance the sensitivity of detection schemes, proposing novel approaches to tackle the minimal current variations associated with these faults. Similarly, in [10,11], the authors emphasize the need for advanced algorithms to detect interturn faults that traditional schemes struggle to identify due to the inherent limitations of differential and *REF* elements.

Expanding on this work, Mohammad et al. [12] and Almeida et al. [13] investigated the use of alternative protection functions, such as directional and sequence-based methods, to improve fault detection accuracy in reactors. These studies demonstrated promising results, particularly in scenarios with a high leakage factor or minimal short-circuited turns, where conventional methods prove inadequate. Furthermore, in [14], the authors provide insights into applying distance functions for fault detection, illustrating their reliability in precisely capturing critical fault conditions.

A turn-to-turn internal fault detection approach was presented in [15] for three-phase wye-connected shunt reactors. In this case, the authors used a time-domain approach sensitive to low-level faults. The unbalanced component is determined by the difference between the measured current and the balanced current in each phase. To obtain the balanced component, the zero-sequence component is subtracted from the phase current calculated in the time domain. Under normal operating conditions of the shunt reactor, the unbalanced current is zero, whereas it becomes nonzero in the presence of an internal fault. Since the phase current is derived from the terminal voltage and the equivalent inductance of each phase, the proposed method remains effective even when system voltage changes.

Zhang et al. [16] implemented finite element simulation models applied to dry-type air core shunt and series reactors. The authors simulated short-circuit faults at various winding layers and positions, thoroughly examining how interstrand and interlayer short circuits affect the equivalent resistance, impedance, and power factor of the reactors. The findings reveal that series reactors are considerably more sensitive to interturn short circuits than shunt reactors, particularly when faults occur at the winding ends. Furthermore, the study shows that interstrand short circuits have a greater impact on electrical parameters than interlayer short circuits.

A detailed analysis and simulation of turn-to-turn faults in shunt reactors, including the algorithms for their detection, was developed in [17]. In this case, the authors present an equivalent circuit model for a shunt reactor, designed to represent faults involving a small number of short-circuited turns. The study explains why conventional differential relays fail to detect turn-to-turn faults effectively. To address this limitation, three detection algorithms were proposed and evaluated under simulated internal fault conditions. These methods rely on zero-sequence reactance, negative-sequence reactance, and phase impedance. The authors also present a detailed assessment of the sensitivity and reliability of each proposed approach.

Turn-to-turn faults create very small changes in the currents and voltages that the relay measures, and therefore, their detection has been a challenging task for engineers. Zhang et al. [18] presented a new algorithm for detecting turn-to-turn faults in shunt reactors. Such an approach uses the negative sequence and the positive sequence voltage and current measurements to develop a differential scheme to sensitively detect internal faults. The proposed approach is able to identify both the turn-to-turn faults and the faulted phases simultaneously.

The research by Almeida et al. [19] stands out for its focus on distance function utilization as the primary protection mechanism. Their findings revealed that distance functions effectively address the challenges posed by turn-to-ground and turn faults, even under adverse conditions such as low fault currents and high leakage factors. This work reinforces the potential of distance functions to enhance reactor protection schemes beyond traditional backup roles.

1.3. Contributions and Paper Outline

The present study contributes to the existing body of knowledge by proposing a comprehensive model to evaluate protection schemes for shunt reactors. By leveraging the mathematical analysis developed for transformers [20], this study adapts the BCTRAN routine for shunt reactor modeling using the three-phase RL Coupled element in ATPDraw software. The proposed model considers parameters such as the number of short-circuited turns and the leakage factor to calculate inductances and resistances under fault conditions. Unlike previous models, this approach specifically addresses the characteristics of dry-type air core shunt reactors, ensuring high accuracy in fault simulations.

This paper is organized as follows: Section 2 presents the theoretical framework and operational principles of the evaluated protection algorithms, including REF, Directional (32Q), Differential (87), and Distance (21) functions. Section 3 describes the methodology and modeling techniques employed for fault simulations using ATPDraw software, highlighting the consideration of parameters such as the leakage factor and the number of short-circuited turns. Section 4 discusses the simulation results, including both transient and parametric sensitivity analyses, and evaluates the performance of each protection function under various fault scenarios. Finally, Section 5 concludes the study with key findings and practical recommendations for enhancing the reliability and efficiency of shunt reactor protection schemes.

2. Implementation and Operation of the Evaluated Protection Algorithms

The protection schemes discussed in this section represent algorithms commonly implemented for reactor protection, as provided by manufacturers to comply with various grid code requirements. These include the *REF* function with blocking elements, the Directional function (32Q), and Differential Protection (87). Additionally, the Distance function (21), traditionally employed as a backup protection mechanism, is examined. Notably, recent findings, such as those in [19], highlight its strong performance as a primary protection solution. The primary aim of this section is to conduct a comparative evaluation of the effectiveness and operational characteristics of these protection schemes.

2.1. Restricted Earth Fault Function (REF)

In this paper, the *REF* logic considered is based on the approach described in [21], which incorporates blocking elements to prevent incorrect *REF* function operations during faults that do not involve the ground. The logical framework of the *REF* algorithm is illustrated in the block diagram shown in Figure 1, comprising Interlock Element1, Interlock Element2, a Directional Element, a Nondirectional Element, and the *REF* TRIP Block. In particular, as shown in Figure 1, the zero-sequence current $\widehat{I}_0$ is calculated using the currents measured by the phase CTs on the terminal side of the phase ($\widehat{I}_A$, $\widehat{I}_B$, and $\widehat{I}_C$), as defined in Equation (1). Additionally, the neutral current $\widehat{I}_n$ is measured by the neutral CT.

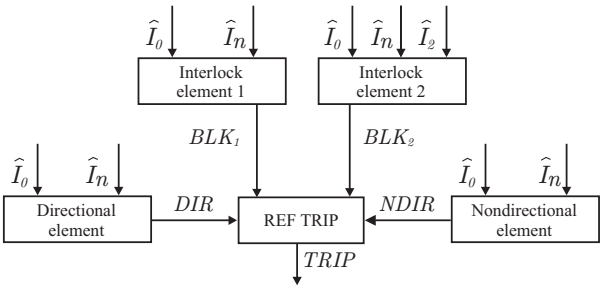

Figure 1. Block diagram of *REF* algorithm.

The inputs to Interlock Element1 are $\widehat{I}_0$ and $\widehat{I}_n$, which are used to determine the zero-sequence current angle θ_0 and the neutral current angle θ_n, respectively. Within this block, k_{REF} serves as the adjustment factor for the *REF* function. If the conditions specified in Equations (2) and (3) are met simultaneously, the variable BLK_1 is activated, taking a value of 1.

$$\widehat{I}_0 = \widehat{I}_A + \widehat{I}_B + \widehat{I}_C \tag{1}$$

$$|\theta_0 - \theta_n| > 105^\circ \tag{2}$$

$$|\widehat{I}_n| > k_{REF}, \qquad |3\widehat{I}_0| > 0.8 \cdot k_{REF} \tag{3}$$

For Interlock Element2, the negative sequence current $\widehat{I}_2$ is used as an input alongside $\widehat{I}_0$ and $\widehat{I}_n$. It is important to note that $\widehat{I}_2$ is calculated using the phase currents $\widehat{I}_A$, $\widehat{I}_B$, and $\widehat{I}_C$, as defined in Equation (4). Within this block, the conditions outlined in Equation (5) are assessed, and if both conditions are satisfied, the variable BLK_2 is activated, taking on a value of 1.

$$\widehat{I}_2 = \frac{1}{3}(\widehat{I}_A + a^2\widehat{I}_B + a\widehat{I}_C) \tag{4}$$

$$max(|\widehat{I}_n, \widehat{I}_0) < 0.1 \cdot |3\widehat{I}_2|, \qquad |3\widehat{I}_2| > k_{REF} \tag{5}$$

If at least one of the variables, BLK_1 or BLK_2, is equal to 1, it indicates the presence of faults that do not involve the ground. In such cases, the *REF* function is blocked and

does not operate for the fault. Conversely, when faults involving the ground occur, the *REF* function is enabled and can operate through either the Directional Element or the Nondirectional Element.

The inputs to both the Directional Element and the Nondirectional Element are $\widehat{I}_0$ and $\widehat{I}_n$. The Directional Element operates when there is sufficient $3\widehat{I}_0$ and the conditions specified in Equations (6) and (3) are met. When these conditions are satisfied, the variable DIR is activated and assigned a value of 1. In contrast, the Nondirectional Element is triggered when there is insufficient $3\widehat{I}_0$ and the conditions described in Equation (7) are met, resulting in the activation of the variable $NDIR$, which is then set to 1.

$$|\theta_0 - \theta_n| < 105^\circ \tag{6}$$

$$|\widehat{I}_n| > k_{REF}, \qquad |3\widehat{I}_0| < 0.8 \cdot k_{REF} \tag{7}$$

Finally, the *REF* TRIP Block sends a trip for faults involving ground, if both BLK_1 and BLK_2 are equal to 0 and DIR or $NDIR$ is equal to 1.

2.2. Directional Function (32Q)

To identify turn faults, a directional function logic similar to those described in [7,22] is implemented. The operation of the 32Q function relies on negative-sequence components: current $\widehat{I}_2$, voltage $\widehat{V}_2$, and impedance Z_2. The voltage $\widehat{V}_2$ is calculated based on the phase voltages $\widehat{V}_A$, $\widehat{V}_B$, and $\widehat{V}_C$. The ratio between $\widehat{V}_2$ and $\widehat{I}_2$ defines Z_2. Additionally, this function utilizes the positive-sequence current $\widehat{I}_1$, which is derived from the currents measured by the phase CTs installed at the phase terminal side, as shown in Equation (8).

This function can be divided into two elements: the forward directional element (32Q_F) and the reverse directional element (32Q_R). The 32Q_F element, responsible for detecting internal reactor faults, operates when the conditions described in Equation (9) are satisfied. Here, k_{ZF} represents the forward impedance threshold, k_{CF} is the current adjustment for internal faults, and k_a evaluates whether the ratio between $\widehat{I}_2$ and $\widehat{I}_1$ exceeds the reactor's natural unbalance.

Conversely, the 32Q_R element, which detects external reactor faults, operates when the conditions described in Equation (10) are met. In this case, k_{ZR} represents the reverse impedance threshold, while k_{CR} corresponds to the current adjustment for external faults. Both k_{ZF} and k_{ZR} are defined in Equation (11), where Z_R denotes the impedance of the reactor.

$$\widehat{I}_1 = \frac{1}{3}(\widehat{I}_A + a\widehat{I}_B + a^2\widehat{I}_C) \tag{8}$$

$$|Z_2| < k_{ZF}, \qquad |3\widehat{I}_2| > k_{CF}, \qquad |\widehat{I}_2/\widehat{I}_1| > k_a \tag{9}$$

$$|Z_2| > k_{ZR}, \qquad |3\widehat{I}_2| > k_{CR}, \qquad |\widehat{I}_2/\widehat{I}_1| > k_a \tag{10}$$

$$k_{ZF} = |Z_R|/2, \qquad k_{ZR} = k_{ZF} + 0.1 \tag{11}$$

To prevent operation during external faults or energization, the negative-sequence element can be intentionally delayed, as suggested in [23]. This delay ensures that a trip is only confirmed if the condition remains active a few milliseconds after its initial detection. In this study, following the adjustment described in [7], a delay of 1.5 cycles was applied to the operation of the 32Q_F element.

2.3. Differential Function (87)

To detect phase faults, this article employs a differential function algorithm that is similar to the solution described in [24]. This algorithm is implemented on a per-

phase basis and compares the currents measured by CT_A, CT_B, and CT_C installed on the phase terminals, with those measured by CT_{AN}, CT_{BN}, and CT_{CN} installed on the neutral terminals. This setup results in two CTs per phase, as illustrated in Figure 2.

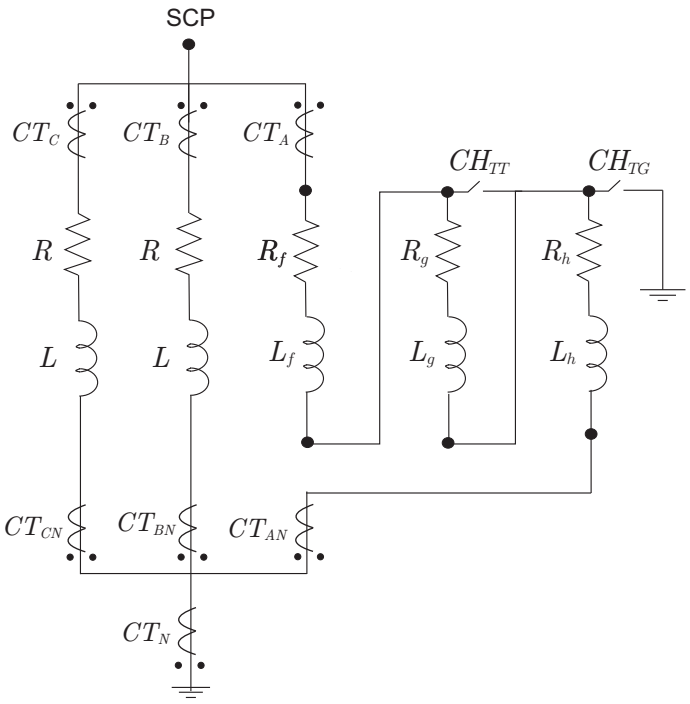

Figure 2. Reactor modeling with the RL Coupled element.

For each phase, an operating current $I_{op\phi}$ and a restraint current $I_{res\phi}$ are determined, as expressed in Equation (12). Here, ϕ represents phases A, B, and C, while $\widehat{I}_{\phi N}$ denotes the currents measured by the CTs installed on the neutral terminals.

$$I_{op\phi} = |\widehat{I}_{\phi} - \widehat{I}_{\phi N}|, \qquad I_{res\phi} = |\widehat{I}_{\phi} + \widehat{I}_{\phi N}| \tag{12}$$

Once the $I_{op\phi}$ and $I_{res\phi}$ currents have been calculated, the 87 function operates when the conditions described in Equation (13) are met, where $Pickup_{87}$ and SPL are the adjustment of the differential function. Once the currents $I_{op\phi}$ and $I_{res\phi}$ have been calculated, the 87 function operates when the conditions described in Equation (13) are satisfied. Here, $Pickup_{87}$ and SPL represent the settings of the differential function.

$$I_{op\phi} > Pickup_{87}, \qquad I_{op\phi} > SLP \cdot I_{res\phi} \tag{13}$$

2.4. Distance Function (21)

To detect turn-to-ground and turn faults, this article employs the distance algorithm described in [19], which is based on an mho phase comparator. Additionally, the sequence voltage memory filter is implemented to define the memorized voltage for each phase, which is denoted as $\widehat{V}_{m\phi}$.

Using the positive-sequence voltage memory filter, the operating voltage ($\widehat{V}_{op\phi}$) and polarization voltage ($\widehat{V}_{pol\phi}$) phasors are determined, as shown in Equations (14) and (15), respectively. Here, $\widehat{V}_{\phi}$ represents the voltage phasor for phase ϕ; h denotes the total impedance of the reactor expressed as a percentage of the protected zone; θ_{Z_R} is the angle of Z_R; and τ corresponds to the design angle of the mho characteristic, also known as the maximum torque angle of the relay.

$$\widehat{V}_{op\phi}(k) = -\widehat{V}_{\phi}(k) + \frac{hZ_R}{\cos(\theta_{Z_R} - \tau)}\widehat{I}_{\phi}(k) \tag{14}$$

$$\widehat{V}_{pol\phi}(k) = \widehat{V}_{m\phi}(k) \tag{15}$$

The phase comparator analysis is performed based on the angle θ_ϕ, which is determined according to Equation (16). Here, $\theta_{op\phi}$ represents the angle of $\widehat{V}_{op\phi}$, and $\theta_{pol\phi}$ represents the angle of $\widehat{V}_{pol\phi}$. For the 21 function to detect the fault, the angle θ_ϕ must be less than 90°; otherwise, its operation will be restrained.

$$\theta_\phi = |\theta_{op\phi} - \theta_{pol\phi}| \tag{16}$$

3. Shunt Reactor Model

Shunt reactors are understood as coils and can be represented by resistors in series with inductors. In this paper, the shunt reactors were modeled considering the theory described in [20], which was originally formulated for power transformers. This modeling approach is valid because power transformers and reactors share similar operating characteristics. Consequently, the mathematical equation presented in [20] can be adapted for application to reactors and implemented in the ATPDraw software, enabling the analysis of turn-to-ground or turn faults.

Hence, to simulate turn-to-ground or turn faults in ATPDraw software, the faulted phase of the reactor is represented through the RL Coupled element, and the remaining phases of the reactor are composed of an inductance in series with a resistor, as shown in Figure 2, where SCP is the system connection point, and the CT_A, CT_B, and CT_C are the CTs on phases A, B, and C, respectively, installed in the phase terminal side. Also, the CT_{AN}, CT_{BN}, and CT_{CN} are the CTs on phases A, B, and C, respectively, installed in the neutral terminal side, and finally, CT_N is the neutral CT installed in the neutral reactor.

For nominal conditions, the total impedance of the healthy phase of the reactor, with 100% of turns equal to n_T, is formed by the resistance R and the self-inductance L. Furthermore, it should be emphasized that, under normal operating conditions, the switches CH_{TT} and CH_{TG} remain open such that the three sub-windings are in series, and the sum of their self- and mutual inductances is equal to the total inductance L of a phase.

In the mathematical formulation considered, for the application of turn faults, the faulted phase winding (e.g., phase A, as shown in Figure 2) must be divided into three parts. The first sub-winding, with n_f percent of turns, is formed by the resistance R_f and the self-inductance L_f; the second sub winding, with n_g percent of turns, is formed by the resistance R_g and the self-inductance L_g; and the third sub-winding, with n_h percent of turns, is formed by the resistance R_h and the self inductance L_h.

To apply a turn fault in phase A, the CH_{TT} switch must be closed such that the fault current (I_F) flows through the first and third sub-winding, as shown in Figure 3. Then, the second sub-winding, with number of turns calculated as $n_g = n_T - n_f - n_h$, is short-circuited so that no current passes by it.

In this model, the fault current is influenced by the leakage factor, which is a constant that varies from zero to one and measures how much the fault current disperses during a fault. The higher the leakage factor, the lower the fault current, and therefore, the operation of the protection function becomes more difficult. The leakage factor depends on the constructive aspects of the reactor and the percentage of turns involved. Thus, for turn faults, three leakage factors are considered to represent this fact: α_{fg}, which measures the coupling between the sub-windings f and g; α_{gh}, which measures the coupling between the sub-windings g and h; and α_{fh}, which measures the coupling between the sub-windings f and h. These factors can be calculated using the equations presented in [20].

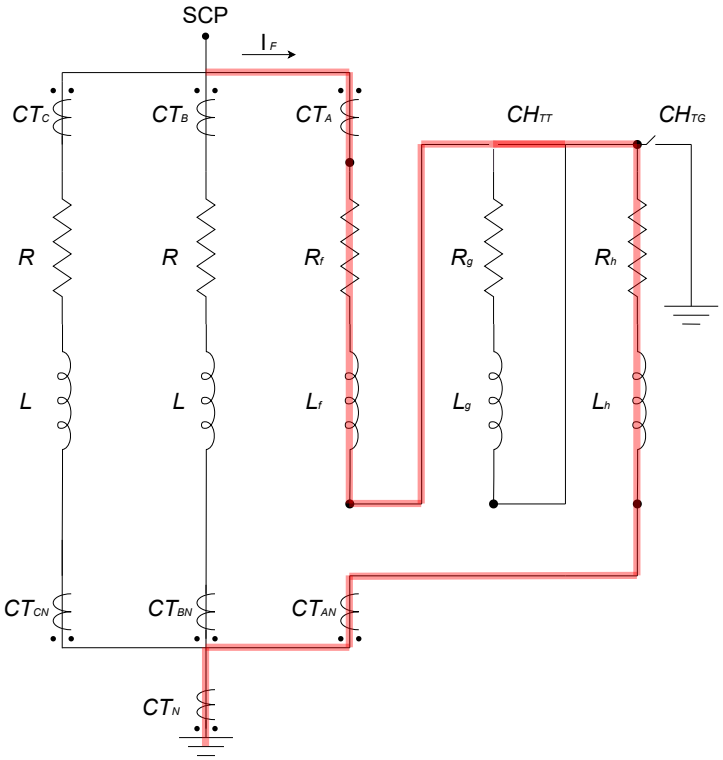

Figure 3. Representation of turn faults.

Considering the need for a unified model capable of simulating both turn-to-turn and turn-to-ground faults, with the latter type requiring closing both the CH_{TG} and CH_{TT} switches. This configuration ensures that the fault current flows exclusively through the first sub-winding, composed of the series arrangement of R_f and L_f, to earth to prevent it from flowing through the other sub-windings, as shown in Figure 4. In this case, the relation between the sub-winding can be defined as $n_g = n_T - n_f$, and only the leakage factor α_{fh} is used.

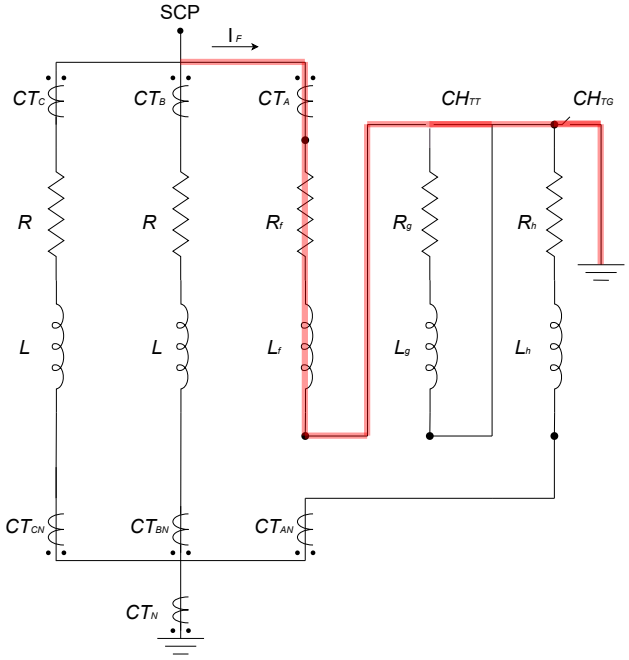

Figure 4. Representation of turn-to-ground faults.

Furthermore, for both turn-to-ground and turn faults, it is acceptable to disregard the mutual coupling between the healthy phases and the faulted phase, since normally the dry-type shunt reactors with an air core are manufactured single-phase and then connected. Therefore, due to its construction, there is a spacing between the phases, which results in better insulation between them and, consequently, less coupling.

4. Tests and Results

To perform the comparative evaluation of the protection functions discussed in Section 2, different operating conditions were simulated using ATPDraw software.

The simulations were based on the power system model illustrated in Figure 5, which consists of a 500 kV/60 Hz transmission line with a length of 400 km and 60% shunt compensation. This compensation, represented as the BR elements in Figure 5, is achieved using two dry-type air core shunt reactors, each with an impedance of $40 + j1718.86\ \Omega$, installed at both ends of the transmission line.

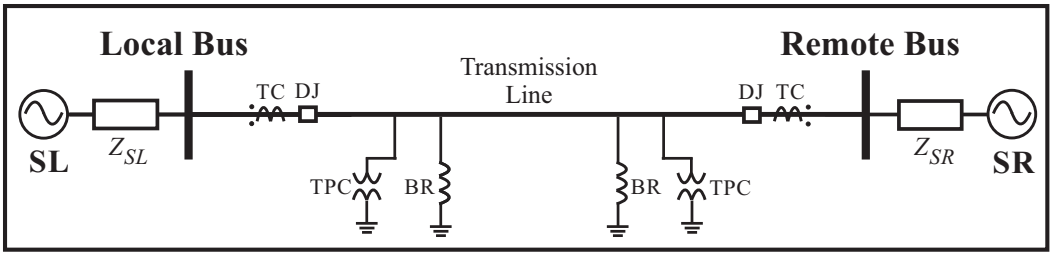

Figure 5. Evaluated power system model.

For the evaluation of protection functions, the first step involves performing transient analyses, where the behavior of the protection functions is assessed during transients. Subsequently, parametric sensitivity analyses are conducted, in which the protection functions are evaluated under a fault steady-state regime. This approach enables the assessment of the influence of the number of short-circuited turns on the performance of the investigated logic. In both analyses, comparative evaluations were performed to identify which functions operate under each described condition. In this context, the evaluations were carried out by analyzing whether a trip signal was issued for each fault condition using different figures that represent the logical state of the trip variables. The abbreviations of the implemented functions are shown on the y axis: 21 is the distance function; 87 is the differential function; *REF* is the Restricted Earth Fault function; $32Q_F$ is the forward directional element; and $32Q_R$ is the reverse directional element.

The x axis represents time in milliseconds for transient analyses. For parametric sensitivity analyses, the x axis indicates the percentage of turns involved in the fault. Furthermore, to implement the described protection logics, the adjustment values were defined based on the references cited for each function [19,21,22,24]. These values correspond to $k_{REF} = 0.0013$ (equal to 0.06 multiplied by the nominal current per phase divided by the neutral nominal current and the neutral CT transformation ratio), $k_{CF} = k_{CR} = 0.05$, $k_a = 0.02$, $Pickup_{87} = 0.3$, $SLP = 0.35$, and $h = 0.9$, which was set equal to the reactor impedance angle. It is noteworthy that, for turn fault simulations, the three leakage factors were considered equal and labeled as α_{tt}.

4.1. Transient Analyzes

For all scenarios evaluated in the transient analyses, faults were applied at 100 ms, and their characteristics are described in Table 1. The operating times of the analyzed functions for each case are presented in Table 2, where an X represents nonoperation.

Table 1. Features of the evaluated faults for transient analyzes.

Case	Description
1	Energization
2	Energization with AG phase-to-ground fault
3	AG Phase-to-ground fault, evolving entire winding
4	AC Phase-to-phase fault, evolving entire winding
5	BC Phase-to-phase fault with 40% of faulted phases short-circuited
6	BC Phase-to-phase fault with 90% of faulted phases short-circuited
7	Turn-to-ground fault with 30% of turn short-circuited and $\alpha_{fh} = 0.7$
8	Turn-to-ground fault with 70% of turn short-circuited and $\alpha_{fh} = 0.3$
9	Turn-to-turn fault with 20% of turn short-circuited and $\alpha_{tt} = 0.6$
10	Turn-to-turn fault with 80% of turn short-circuited and $\alpha_{tt} = 0.8$
11	AB Two-phase external fault
12	BT Phase-to-ground external fault
13	ABC Three-phase external fault with the CT saturation of three phases
14	AT Phase-to-ground external fault with the CT saturation of phase A

Table 2. Protection function operating time in milliseconds.

Case	t_{21}	t_{87}	t_{REF}	t_{32QF}	t_{32QR}
1	*X*	*X*	16.70	*X*	*X*
2	1.07	0.03	1.07	25.03	*X*
3	1.07	1.07	0.03	25.03	*X*
4	1.07	1.07	*X*	25.03	*X*
5	13.58	6.28	*X*	27.12	*X*
6	3.16	3.16	*X*	26.07	*X*
7	1.07	1.07	1.07	26.07	*X*
8	2.12	1.07	1.07	26.07	*X*
9	3.16	*X*	*X*	26.07	*X*
10	1.07	*X*	*X*	26.07	*X*
11	10.45	*X*	*X*	*X*	1.07
12	12.54	*X*	*X*	*X*	4.20
13	15.67	1.07	3.16	*X*	1.07
14	15.67	1.07	*X*	*X*	5.24

To evaluate whether the protection functions operated during an energization maneuver, Case 1 was analyzed, where the reactor was energized at 100 ms. For this case, the behavior of the currents measured at the reactor phase terminals is shown in Figure 6, which presents the current behavior between 50 ms and 1000 ms. Note that before energization, the current values were zero. Following energization at 100 ms, the currents exhibited different values across the phases, resulting in an unbalance that persisted until

approximately 750 ms. However, after this initial transient state, the currents stabilized and became balanced in the steady-state regime, as shown in Figure 7, which corresponds to the time interval between 750 ms and 1000 ms.

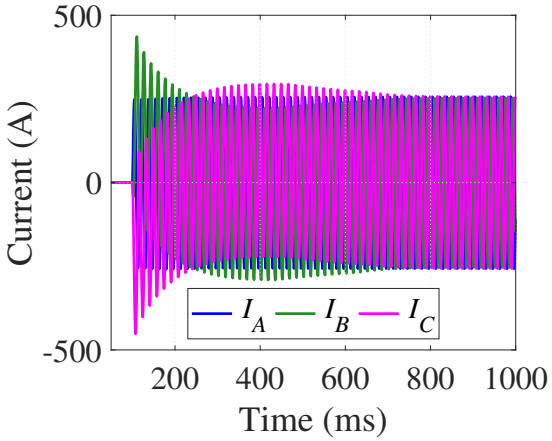

Figure 6. Current performance during energization (Case 1): 50–1000 ms.

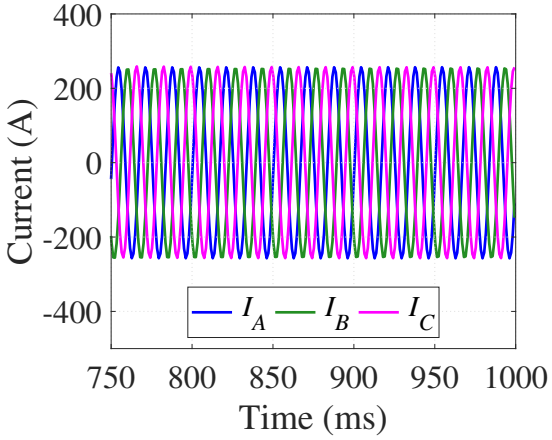

Figure 7. Current performance during energization (Case 1): zoomed-in range between 750 ms and 1000 ms.

As shown in Figure 8, which presents the state variable trips between 100 ms and 1000 ms, the *REF* element was activated due to the unbalance caused during energization, where the zero-sequence currents were not zero. In the steady-state regime (after 750 ms), it is noted that none of the protection functions were activated.

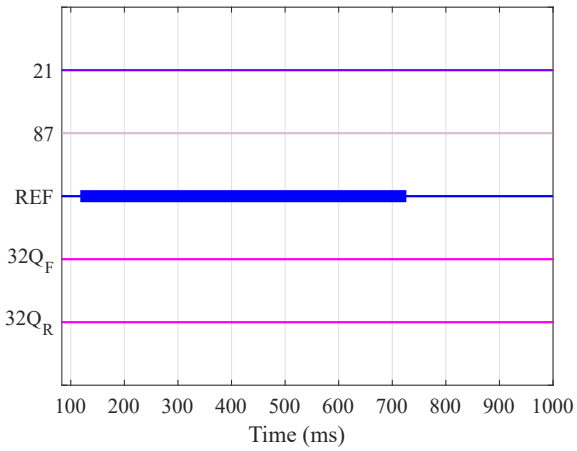

Figure 8. Variable TRIP state for Case 1.

The reactor energization with an AG phase-to-ground fault was evaluated in Case 2, and the results are presented in Figure 9. It can be observed that all functions operated, except for the $32Q_R$ element, which operated only for external faults. According to Table 2, the 87 function had the fastest operation, while the $32Q_F$ function had the slowest operation due to the applied delay.

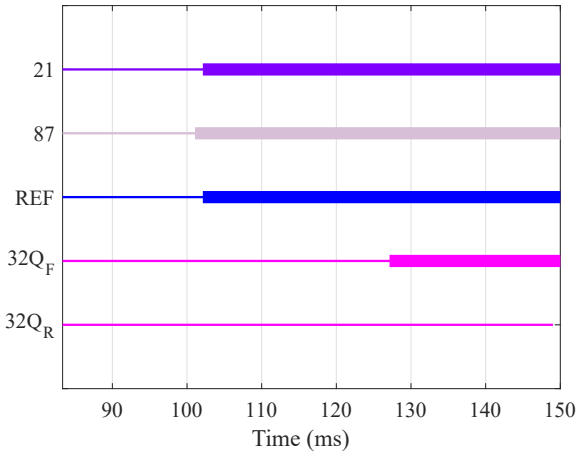

Figure 9. Variable TRIP state for Case 2.

Based on Table 1, Case 3 corresponds to an AG phase-to-ground fault involving the entire winding of phase A. The results are presented in Figure 10. Note that all functions operated, except for the $32Q_R$ element, as there was no external fault. According to Table 2, the *REF* function had the shortest operating time, while the $32Q_F$ function had the longest operating time due to the implemented delay.

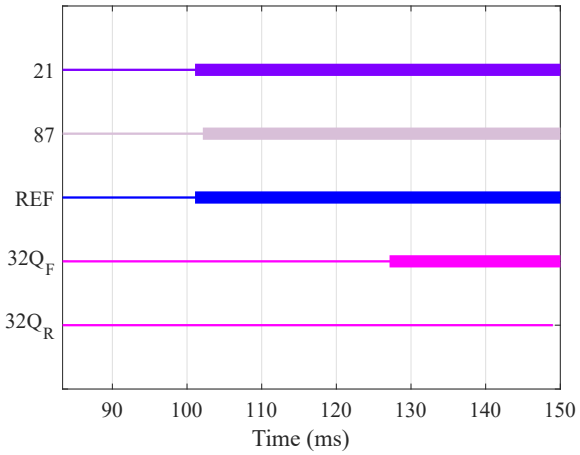

Figure 10. Variable TRIP state for Case 3.

Based on Table 1, Case 4 corresponds to a phase-to-phase fault involving phases A and C. The results are presented in Figure 11, where it is observed that *REF* and $32Q_R$ functions did not operate. This outcome is expected, as these functions are not designed to operate for internal faults that do not involve ground. According to Table 2, the 21 and 87 functions had the shortest operating times, while the $32Q_F$ function had the longest operating time due to the implemented delay.

Figures 12 and 13 present the results for Cases 5 and 6, respectively, which correspond to phase-to-phase faults with 40% and 90% of the short-circuited faulted phases, respectively. Note that functions *REF* and $32Q_R$ did not operate, as these are internal faults that do not involve the ground. On the other hand, functions 21, 87, and $32Q_F$ operated. According to Table 2, for both Cases 5 and 6, the 87 function had the shortest operating time, while

the $32Q_F$ function had the longest operating time. When comparing Cases 5 and 6, it can be seen that the operation in Case 6 was faster, as a larger percentage of turns were short-circuited. Consequently, the fault current was greater, and the protection function was activated more quickly.

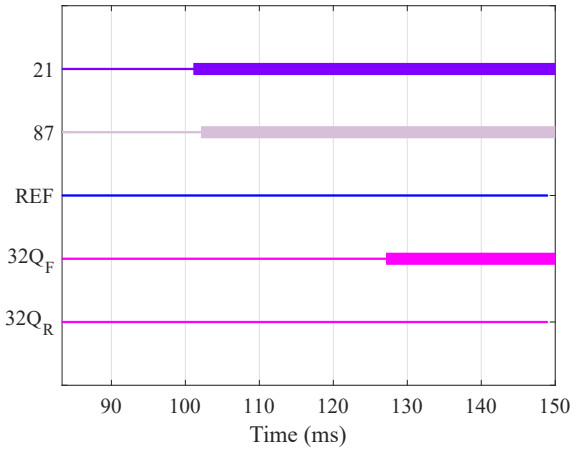

Figure 11. Variable TRIP state for Case 4.

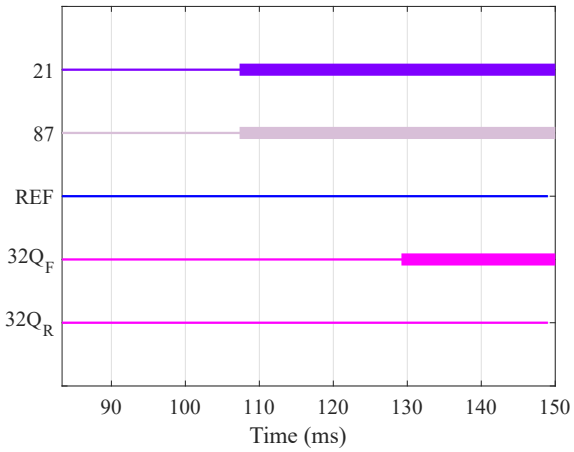

Figure 12. Variable TRIP state for Case 5.

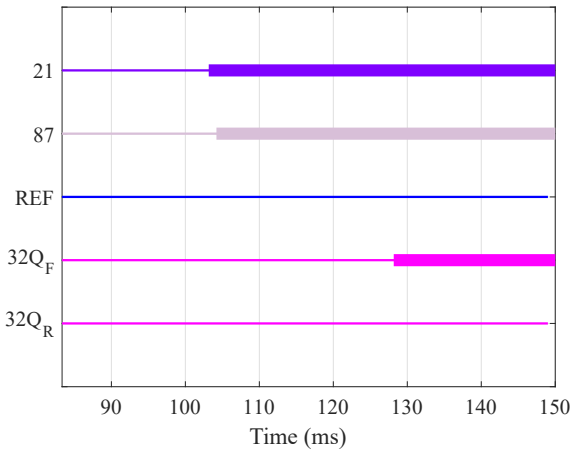

Figure 13. Variable TRIP state for Case 6.

Turn-to-ground faults were evaluated in Cases 7 and 8. In Case 7, with 30% of short-circuited turns and $\alpha_{fh} = 0.7$. In Case 8, with 70% of short-circuited turns and $\alpha_{fh} = 0.3$. The results in both cases are similar and are illustrated in Figure 14, it is observed that the

21, 87, REF, and $32Q_F$ functions operated. The lack of operation of the $32Q_R$ element is justified, as there was no external fault.

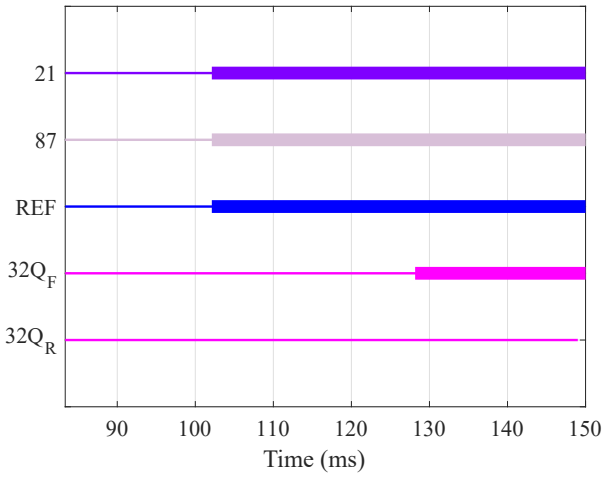

Figure 14. Variable TRIP state for Case 7 and Case 8.

According to Table 2, we have the following: (1) In Case 7, the 21, 87, and *REF* functions had the shortest operating times. (2) In Case 8, the 87 and *REF* functions had the shortest operating times. For both Cases 7 and 8, the 87 and *REF* function had the longest operating time.

Cases 9 and 10 correspond to turn faults with 20% with $\alpha_{tt} = 0.6$ and 80% of short-circuited turns with $\alpha_{tt} = 0.8$, respectively. The results in both cases are similar and are illustrated in Figure 15.

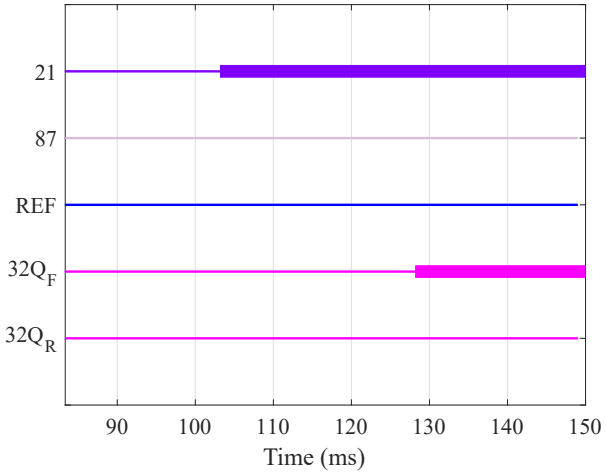

Figure 15. Variable TRIP state for Case 9 and Case 10.

Based on these results, it is observed that the behavior of the functions was similar for both cases, with only the 21 and $32Q_F$ functions operating. According to Table 2, for both Cases 9 and 10, the 21 function had the shortest operating time, while the $32Q_F$ function had the longest operating time. In these cases, the magnitudes of the currents measured at the phase and neutral terminals were the same; however, the current phasors were shifted by 180°, which explains the nonoperation of the 87 function. Additionally, the *REF* function did not operate because these faults do not involve ground.

In order to verify the reliability of the evaluated protection functions, several cases of external faults were analyzed. For these simulations, the system shown in Figure 5 was modified so that two identical transmission lines, each 230 km long, were connected upstream of the local bus. On one of these lines, a three-phase external fault

(Case 11) and a BG phase-to-ground external fault (Case 12) were simulated 5 km away from the local bus. These external faults were intentionally applied close to the reactor; however, their occurrence should not trigger the reactor protection functions.

The results for the external fault of two phases and the external fault of AG phase to ground are presented in Figures 16 and 17, respectively. In both Cases 11 and 12, it is observed that the $32Q_R$ function operated as expected, given that these are external faults. However, and in both cases, the 21 function operated briefly for a few milliseconds. To prevent this transient operation of the distance function, the reach of the distance zone (parameter h in Equation (14)) can be reduced. This adjustment prevents the distance protection from malfunctioning during external faults.

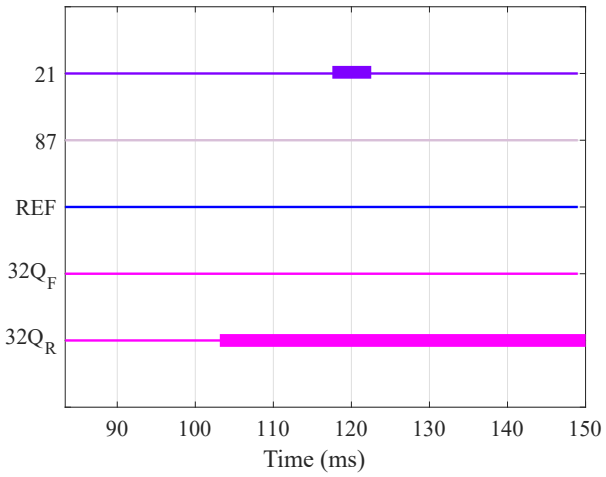

Figure 16. Variable TRIP states for Case 11.

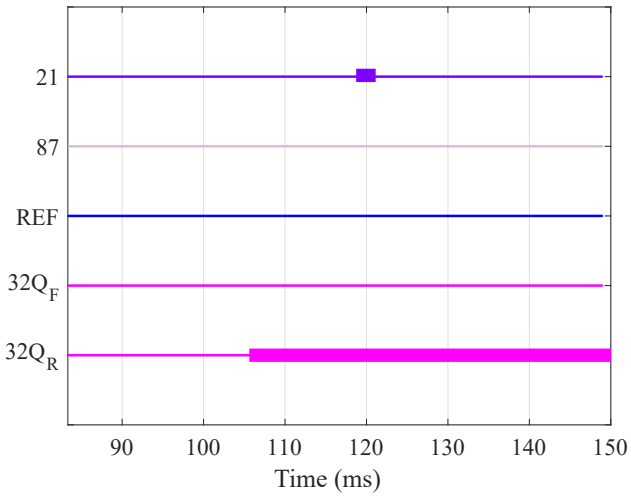

Figure 17. Variable TRIP states for Case 12.

Regarding external faults, it is also necessary to evaluate the occurrence of CT saturation, as the combination of these two events can result in incorrect protection operation. In this context, Case 13 was simulated, representing an external three-phase fault that led to the saturation of the three CTs installed on the phase terminal side (indicated in Figure 2 as CT_A, CT_B and CT_C). Furthermore, Case 14 was simulated, corresponding to an external AG phase-to-ground fault that caused saturation of CT_A, as indicated in Figure 2.

The results of Cases 13 and 14 are shown in Figures 18 and 19, respectively. In both cases, it is observed that the $32Q_R$ functions operated as expected, as they correspond to external faults. In Case 13, the 87 element failed, while in Case 14, the 59 element did not operate correctly. During these two external faults, the 21 and 87 functions were active for

a few milliseconds. To prevent this transient operation of the distance function, the reach of the distance zone (parameter h in Equation (14)) can be reduced, thus avoiding distance protection malfunctions during external faults.

Lastly, regarding the performance of the 21 function, it is important to emphasize that although this function exhibited transient operation during the simulated external faults, an evaluation of its operating time revealed that tripping would require more than 10 ms to occur. Within this interval, the external fault would most likely be cleared, meaning that the 21 function would not actually trip, even temporarily. Therefore, it can be concluded that immediately after the fault occurs, the 21 function remains inactive, ensuring the secure operation of this protection function.

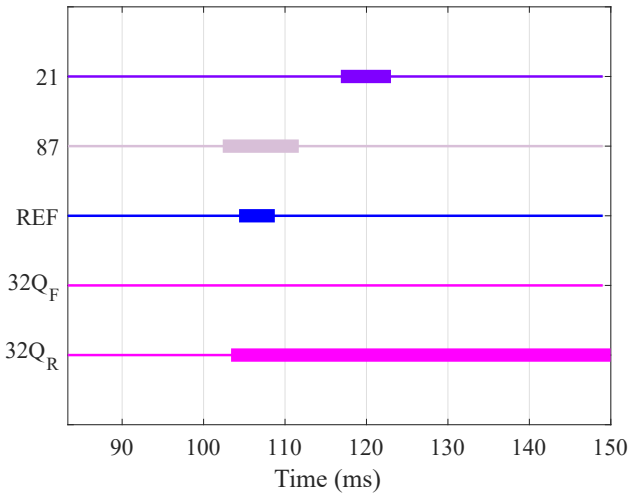

Figure 18. Variable TRIP states for Case 13.

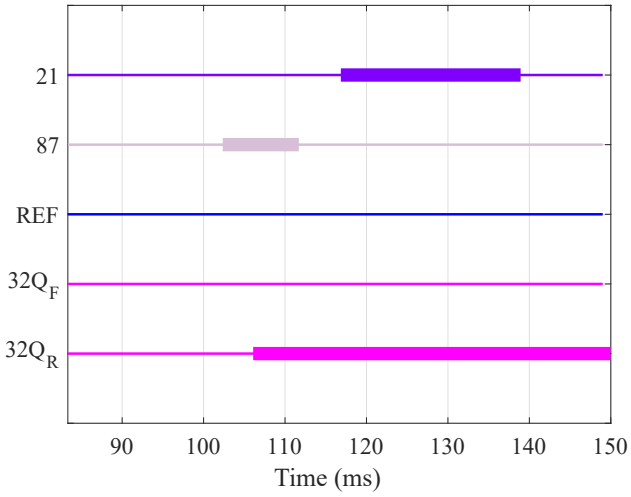

Figure 19. Variable TRIP states for Case 14.

4.2. Parametric Sensitivity Analyzes

To assess the influence of the number of short-circuited turns on the performance of protection functions, parametric sensitivity analyses were employed. These analyses allow for the consideration of this variation, enabling more comprehensive evaluations. For turn-to-ground faults, the number of short-circuited turns ranges from 1% to 99%, while for turn faults, it ranges from 1% to 98%. Across the evaluated cases, a total of 591 faults were simulated in the parametric sensitivity analyses, with their characteristics summarized in Table 3.

Table 3. Features of the evaluated faults for parametric sensitivity analyses.

Case	Type of Fault	Leakage Factor
15	Turn-to-ground	$\alpha_{fh} = 0.01$
16	Turn-to-ground	$\alpha_{fh} = 0.5$
17	Turn-to-ground	$\alpha_{fh} = 1.0$
18	Turn-to-turn	$\alpha_{tt} = 0.01$
19	Turn-to-turn	$\alpha_{tt} = 0.5$
20	Turn-to-turn	$\alpha_{tt} = 1.0$

Cases 15, 16, and 17, which correspond to turn-to-ground faults, presented the same results and are illustrated in Figure 20. Functions 21, 87, REF, and $32Q_F$ operated regardless of the number of turns involved or the leakage factor value.

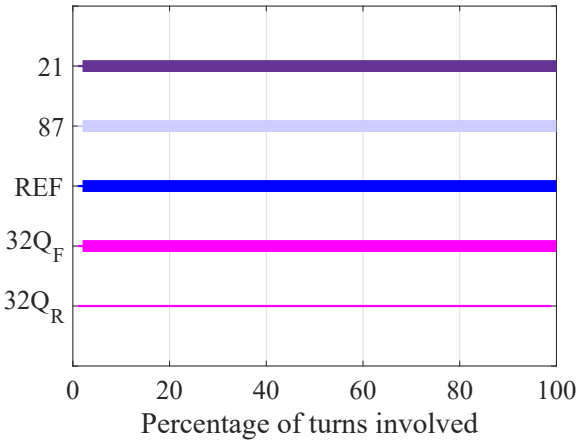

Figure 20. Variable TRIP state for Case 15, 16 and 17

Cases 18 and 19, which correspond to turn faults presented the same results and are illustrated in Figure 21. It is observed that the 21 and $32Q_F$ functions operated regardless of the number of short-circuited turns.

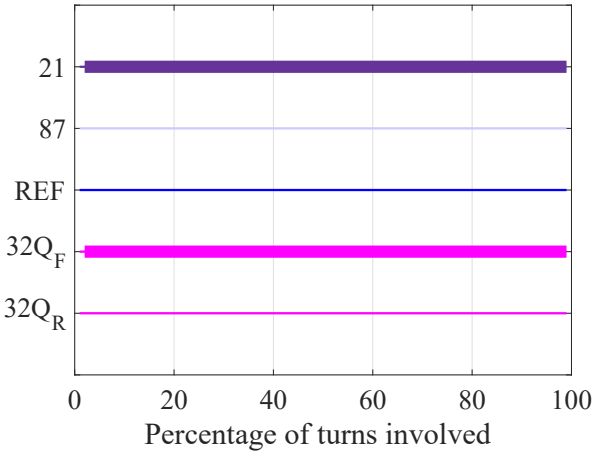

Figure 21. Variable TRIP state for Case 18 and Case 19.

In Case 20, which corresponds to turn faults and is illustrated in Figure 22, the leakage factor was equal to 1.00 ($\alpha_{tt} = 1.0$), resulting in lower fault currents. Consequently, for faults involving a small number of short-circuited turns, the performance of the 21 function was compromised, operating only for faults with more than 14% of short-circuited turns. In contrast, the $32Q_F$ function operated regardless of the number of turns involved.

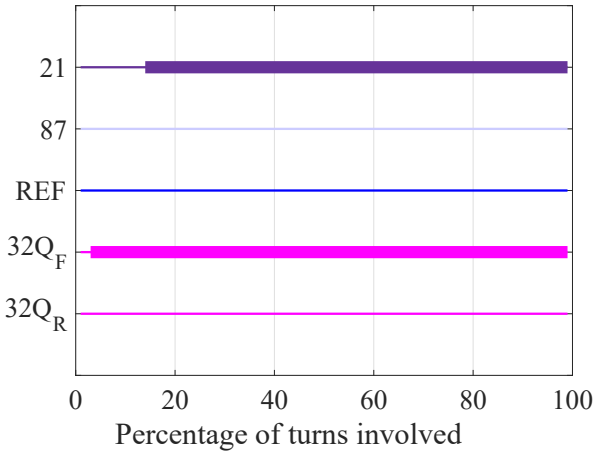

Figure 22. Variable TRIP state for Case 20.

Furthermore, in Cases 18, 19, and 20, as these correspond to turn faults, the magnitudes of the currents measured at the phase and neutral terminals were identical. However, these phasor currents were shifted by 180°, which explains the nonoperation of the 87 function. Finally, similar to what was observed for turn faults in transient analyzes, it is confirmed that the *REF* function did not operate in Cases 18, 19, and 20, as these faults do not involve ground. Furthermore, the $32Q_R$ function did not operate in any of the parametric sensitivity analysis cases because all these faults correspond to internal faults.

4.3. Discussion of Results

Based on the results of the transient and parametric sensitivity analyses, Table 4 summarizes the performance of the analyzed protection functions. The table presents the results for turn-to-ground faults (referred to as TG faults) and turn-to-turn faults (denoted as TT faults), where a ✓ indicates operation, and an *X* represents nonoperation.

Table 4. Summary of operation results.

Function	Transient Analyses		Parametric Sensitivity Analyses	
	TG Fault	TT Fault	TG Fault	TT Fault
87	✓	*X*	✓	*X*
REF	✓	*X*	✓	*X*
21	✓	✓	✓ with exceptions	✓
$32Q_F$	✓	✓	✓	✓

According to the Table 4 and the transient analyses, it is observed that, with the exception of turn faults, the 87 function operated in all cases. Additionally, the *REF* function did not operate for phase-to-phase or turn faults, as these faults do not involve ground. Therefore, the 87 and *REF* functions must be used in conjunction with other protection functions to ensure reliable protection against turn faults. It was also noted that the 21 and $32Q_F$ functions demonstrated the best performance, as they operated correctly in all analyzed cases of internal faults. The 21 function exhibited the shortest operating time (less than one cycle), whereas the $32Q_F$ function was slower due to the intentional delay implemented to prevent incorrect operation during transients. Finally, considering all simulated cases, the $32Q_R$ function operated exclusively for external faults, and the 21 function maintained its security, even during external faults accompanied by CT saturation.

From the the Table 4 and the faults evaluated in the parametric sensitivity analyses, it is observed that the 87 and *REF* functions operated exclusively for turn-to-ground faults. Furthermore, it is noted that the performance of the 21 and $32Q_F$ functions was quite

similar for both turn-to-ground and turn faults. The $32Q_F$ function operated regardless of the number of turns involved or the leakage factor value. Similarly, the 21 function also operated reliably, except in cases of turn faults with a high leakage factor and a small number of short-circuited turns.

It is important to emphasize that the results obtained pertain to a dry-type reactor connected to a transmission line operating at 500 kV and 60 Hz, with 60% shunt compensation. Given the specific characteristics of the evaluated electrical system, the study presents certain limitations in its analysis. Therefore, to achieve a more comprehensive assessment of the analyzed protection functions, it may be beneficial to conduct similar simulations under different operating conditions, such as varying shunt compensation levels, different voltage ratings, and reactors with an iron core.

5. Conclusions

This study presented a comprehensive comparative evaluation of protection schemes for shunt reactors, addressing turn-to-ground and turn faults through transient and parametric sensitivity analyses using ATPDraw software. The results highlight the critical importance of design parameters, specifically the leakage factor and the number of short-circuited turns, in determining the performance of protection functions. Among the analyzed functions, the functions 21 (distance) and $32Q_F$ (directional negative sequence) demonstrated superior overall performance, reliably operating under all internal fault conditions regardless of the evaluated parameters. The 21 function stood out for its shorter operating time, often below one cycle, positioning it as a viable candidate for primary protection. In contrast, the 87 (differential) function showed limitations in scenarios involving faults with a small number of short-circuited turns and high leakage factor values, while the *REF* (Restricted Earth Fault) function proved ineffective for faults that did not involve the ground.

Furthermore, the study identified transient misoperations during external faults with CT saturation, which particularly affected the functions 21 (distance) and 87 (differential). To address this, it was proposed to adjust the reach of the distance zone (parameter h), preventing incorrect activations during transient conditions. In general, the results support the conclusion that the 21 (distance) function, complemented by other traditional protection functions, can serve as an effective primary protection scheme for shunt reactors. This approach significantly improves the reliability and efficiency of protection systems, ensuring robust performance even under challenging fault scenarios. Furthermore, the findings provide practical recommendations for optimizing the implementation of protection schemes in real-world power systems, contributing to the safety and stability of electrical networks.

Author Contributions: Conceptualization, M.L.S.d.A. and D.G.F.; Data curation, M.L.S.d.A. and D.G.F.; Formal analysis, M.L.S.d.A., D.G.F. and L.P.G.N.; Funding acquisition, J.M.L.-L. and N.M.-G.; Investigation, M.L.S.d.A., D.G.F., L.P.G.N., J.M.L.-L. and N.M.-G.; Methodology, M.L.S.d.A., D.G.F. and L.P.G.N.; Project administration, M.L.S.d.A., D.G.F., L.P.G.N., J.M.L.-L. and N.M.-G.; Resources, M.L.S.d.A., D.G.F., L.P.G.N., J.M.L.-L. and N.M.-G.; Software, M.L.S.d.A. and D.G.F.; Supervision, M.L.S.d.A., D.G.F., L.P.G.N., J.M.L.-L. and N.M.-G.; Validation, M.L.S.d.A., D.G.F. and L.P.G.N.; Visualization, M.L.S.d.A., D.G.F., L.P.G.N., J.M.L.-L. and N.M.-G.; Writing—original draft, M.L.S.d.A. and D.G.F.; Writing—review and editing, L.P.G.N., J.M.L.-L. and N.M.-G. All authors have read and agreed to the published version of the manuscript.

Funding: This research was funded by the Colombian Ministry of Science, Technology, and Innovation "MinCiencias" through "Patrimonio Autónomo Fondo Nacional de Financiamiento para la Ciencia, la Tecnología y la Innovación, Francisco José de Caldas" (Perseo Alliance, Contract No. 112721-392-2023) and the National Council for Scientific and Technological Development (CNPq)

through the Chamada CNPq/MCTI/FNDCT No. 18/2021—Faixa A—Emerging Groups—process No. 408898/2021-6.

Data Availability Statement: The data presented in this study are available on request from the corresponding author.

Acknowledgments: The authors gratefully acknowledge the Colombian Ministry of Science, Technology, and Innovation "MinCiencias" through "Patrimonio Autónomo Fondo Nacional de Financiamiento para la Ciencia, la Tecnología y la Innovación, Francisco José de Caldas" (Perseo Alliance, Contract No. 112721-392-2023); and the National Council for Scientific and Technological Development (CNPq) through the Chamada CNPq/MCTI/FNDCT No. 18/2021—Faixa A—Emerging Groups—process No. 408898/2021-6.

Conflicts of Interest: The authors declare no conflicts of interest.

References

1. Njabulo Zwane, S.; Mendu, B.; Baakanyang Monchusi, B. State-of-the-Art Review: Models and Algorithms for Optimal Power System Design, Stabilization, and Reliability Enhancement. *IEEE Access* **2024**, *12*, 189871–189883. [CrossRef]
2. Feng, N.; Feng, Y.; Su, Y.; Zhang, Y.; Niu, T. Dynamic Reactive Power Optimization Strategy for AC/DC Hybrid Power Grid Considering Different Wind Power Penetration Levels. *IEEE Access* **2024**, *12*, 187471–187482. [CrossRef]
3. Javaid, S.; Kaneko, M.; Tan, Y. Energy Balancing of Power System Considering Periodic Behavioral Pattern of Renewable Energy Sources and Demands. *IEEE Access* **2024**, *12*, 70245–70262. [CrossRef]
4. CIGRE. *Protection, Monitoring and Control of Shunt Reactors*; Technical Report; Working Group B5.37; CIGRE: Paris, France, 2012.
5. Li, L.; He, J.; Niu, J.; Liu, H.; Yu, X.; Huang, Y.; Zhang, X. A Phase-to-Phase Protection Algorithm with the Transient Information for the Wind Power Plant Transmission Line. *IEEE Access* **2024**, *12*, 100581–100590. [CrossRef]
6. *IEEE Std C37.109-2006*; IEEE Guide for the Protection of Shunt Reactors—Redline. IEEE: New York, NY, USA, 2007.
7. Chowdhury, R.; Fischer, N.; Taylor, D.; Caverly, D.; Dehkordi, A.B. A Fresh Look at Practical Shunt Reactor Protection. In Proceedings of the 76th Annual Georgia Tech Protective Relaying Conference, Atlanta, Georgia, 3–5 May 2023.
8. Li, Q.; Wang, Z.; Zhao, H.; Dong, J.; Shen, Z.; Zhang, X.; Zhang, Z.; Hu, E.; Xing, Y. Interturn Fault Detection Algorithm for Shunt Reactors Based on Leakage Magnetic Field. In Proceedings of the 2019 IEEE 3rd Conference on Energy Internet and Energy System Integration (EI2), Changsha, China, 8–10 November 2019; pp. 2303–2307. [CrossRef]
9. Uriondo, F.; Aguirre, G.; Hernández, J.; García, J. Improving HV Shunt Reactors REF Relaying. In Proceedings of the 2019 IEEE 3rd Conference on Energy Internet and Energy System Integration (EI2), Changsha, China, 8–10 November 2019.
10. Das, S.; Sidhu, T.; Zadeh, M.R.D.; Zhang, Z. A novel method for turn to turn fault detection in shunt reactors. In Proceedings of the 2017 70th Annual Conference for Protective Relay Engineers (CPRE), College Station, TX, USA, 3–6 April 2017; pp. 1–9.
11. Basha, F.K.; Thompson, M. Practical EHV reactor protection. In Proceedings of the 2013 66th Annual Conference for Protective Relay Engineers, College Station, TX, USA, 8–11 April 2013.
12. Mohammad, A.I.; Mort, T.; Jeter, J.; Hoth, A.; England, J.; Johnson, B.K.; Fischer, N.; Damron, K. Turn-to-Turn Fault Protection for Dry-Type Shunt Reactors. In Proceedings of the 2018 IEEE/PES Transmission and Distribution Conference and Exposition (T&D), Denver, CO, USA, 16–19 April 2018; pp. 1–5.
13. de Almeida, M.L.S.; Peres, L.M.; dos Santos, G.G. Air-core dry-type shunt reactor protection based on an alternative current alpha plane. *IET Gener. Transm. Distrib.* **2021**, *15*, 34–44. [CrossRef]
14. Almeida, M.L.S.; Peres, L.M.; Silva, K.M. On applying an Enhanced Generalized Alpha Plane to shunt reactor protection. *Electr. Power Syst. Res.* **2022**, *212*, 108387. [CrossRef]
15. Mohanty, R.; Pradhan, A.K. Protection for Turn-to-Turn Internal Fault in Shunt Reactors using Time-Domain Approach. In Proceedings of the 2023 7th International Conference on Computer Applications in Electrical Engineering-Recent Advances (CERA), Roorkee, India, 27–29 October 2023; pp. 1–5. [CrossRef]
16. Zhang, H.; Zhang, W.; Jiao, B. Analysis of Inter-Turn Short Circuit Characteristics in the Windings of Dry-Type Air-Core Series and Shunt Reactors. In Proceedings of the 2024 IEEE 7th International Conference on Automation, Electronics and Electrical Engineering (AUTEEE), Shenyang, China, 27–29 December 2024; pp. 452–456. [CrossRef]
17. Solak, K.; Mieske, F.; Schneider, S. Modeling and Detection of Turn-to-Turn Faults in Shunt Reactors. *IEEE Access* **2022**, *10*, 1386–1400. [CrossRef]
18. Zhang, Z.; Makwana, S.; Mysore, P.G.; Nyombi, P.I. Implementation of a new algorithm to detect turn-to-turn faults in shunt reactors and identify the faulted phase. In Proceedings of the 15th International Conference on Developments in Power System Protection (DPSP 2020), Liverpool, UK, 9–12 March 2020; pp. 1–6. [CrossRef]

19. Almeida, M.L.S.; Silva, K.M. An investigation of distance protection function applied for shunt reactors. *Electr. Power Syst. Res.* **2023**, *223*, 109579. [CrossRef]
20. Bastard, P.; Bertrand, P.; Meunier, M. A transformer model for winding fault studies. *IEEE Trans. Power Deliv.* **1994**, *9*, 690–699. [CrossRef]
21. Chowdhury, R.; Alla, M.; Fischer, N.; Samineni, S. Restricted Earth Fault Protection in Low-Impedance Grounded Systems with Inverter-Based Resources. *IEEE Trans. Power Deliv.* **2023**, *38*, 505–512. [CrossRef]
22. McDaniel, R.; Thompson, M. Impedance-Based Directional Elements—Why Have a Threshold Setting. In Proceedings of the 75th Annual Georgia Tech Protective Relaying Conference, Atlanta, GA, USA, 4–6 May 2022.
23. Kasztenny, B.; Fischer, N.; Altuve, H.J. Negative-Sequence Differential Protection—Principles, Sensitivy, and Security. In Proceedings of the 69th Annual Georgia Tech Protective Relaying Conference, Atlanata, GA, USA, 29 April–1 May 2015; Schweitzer Engineering Laboratories Inc.: Pullman, WA, USA, 2014.
24. Chowdhury, R.; Finney, D.; Fischer, N. Determining CT Requirements for Generator and Transformer Protective Relays. In Proceedings of the 74th Annual Conference for Protective Relay Engineers, Virtual, 22–25 March 2021.